

Cite this: *Biomater. Sci.*, 2023, **11**, 5274

Functionalized hydrogel–microsphere composites stimulating neurite outgrowth for vascularized bone regeneration†

Qian Li,^{‡a,b} He Zhang,^{‡a} Ziqian Zeng,^a Shuang Yan,^a Yu Hei,^c Yifei Zhang,^a Yang Chen,^b Siqi Zhang,^d Wen Zhou,^a Shicheng Wei ^{*a,b} and Yuhua Sun^{*e}

Neurovascularized bone regeneration remains an enormous challenge in the clinic. Biomaterials mimicking the developmental microenvironment might be promising tools to enhance tissue regeneration. In this study, functionalized hydrogel–microsphere composites are developed to enhance bone regeneration *via* a recapitulating neurovascularized microenvironment. RGD peptide and the porous structure generated by the degradation of gelatin microspheres (GMs) are beneficial for the proliferation and migration of human mesenchymal stem cells (hMSCs); mesoporous silica nanoparticles (MSNs) promote osteogenic differentiation of hMSCs through the delivery of BFP-1 peptide; the QK peptide from the GMs is sustained-released to recruit endogenous endothelial cells (ECs), and IK19 peptide grafted on the hydrogel guides the neurite outgrowth. The *in vivo* results show that the hydrogel–microsphere composites not only promote new bone formation, but also facilitate nerve infiltration and angiogenesis. Furthermore, the neurovascularized niche created by this composite stimulated neurite growth through MAPK, PI3K, IL17 and TNF signaling pathways, enabling vascularized bone regeneration. The findings suggest a novel bioengineering approach to guide the construction of neurovascularized bone repair materials, which is beneficial for achieving functional bone regeneration and repair.

Received 6th March 2023,

Accepted 1st June 2023

DOI: 10.1039/d3bm00401e

rsc.li/biomaterials-science

1 Introduction

Despite the regenerative capacity of bone tissue, approximately 10% of fracture union failures are due to delayed union or nonunion, and the rate of union failure is as high as 46% if associated with major vascular injury.¹ Although bone tissue engineering has great potential in the repair of bone defects, the lack of timely vascularization has become a major challenge hindering its clinical translation.² Given the lack of blood vessels, the cells inside the graft cannot obtain sufficient oxygen and nutrients. Such cells are prone to apoptosis, limiting the application of bone tissue engineering in large defects.³

Several strategies have been proposed to improve vascularization in bone tissue engineering, such as introducing endothelial cells (ECs) to form a pre-vascularized network, or delivering pro-angiogenic factors (*e.g.*, VEGF) to promote angiogenesis *in vivo*.⁴ We previously prepared a tripeptide-based macroporous alginate hydrogel (RBQ), which released VEGF biomimetic peptide-QK peptide through degradable gelatin microspheres (GMs) to recruit endogenous ECs and sustained-release osteogenic peptide BFP-1 through mesoporous silica nanoparticles (MSNs) to promote the osteogenic differentiation of stem cells. The use of mice transplanted *in vivo* confirmed that RBQ could promote osteogenic differentiation and angiogenesis.⁵

In addition to vascularization, innervation also plays an important role in promoting engineered bone tissue repair.⁶ Patients who lack peripheral innervation experience delayed or nonunion fractures and are at risk of fracture recurrence, primarily because nerve loss reduces the activity of osteoblasts and increases the number and activity of osteoclasts, which are detrimental to bone growth.⁷ In fact, the human skeleton is fully vascularized and innervated, in which blood vessels and nerve fibers closely interact and enhance each other's development and function, ultimately supporting skeletal development and fracture healing.⁸

Although some studies have reported vascularized bone repair systems, few studies have been conducted on innervated

^aDepartment of Oral and Maxillofacial Surgery, Central Laboratory, Peking University School and Hospital of Stomatology, Beijing 100081, China.

E-mail: sc-wei@pku.edu.cn

^bLaboratory of Biomaterials and Regenerative Medicine, Academy for Advanced Interdisciplinary Studies, Peking University, Beijing 100871, China

^cCollege of Engineering, Peking University, Beijing 100871, China

^dInstitute of Molecular Medicine, Peking University, Beijing 100871, China

^eDepartment of Stomatology, the Affiliated Hospital of Xuzhou Medical University, Xuzhou 221004, China. E-mail: yuhua.sun@xzhmu.edu.cn

† Electronic supplementary information (ESI) available. See DOI: <https://doi.org/10.1039/d3bm00401e>

‡ These authors are equal contributors to this work.

bone repair systems.⁷ Several studies have attempted to construct neurovascularized bone grafts by microsurgically integrating vascular bundles and nerve fibers onto the graft.⁹ Xu *et al.* have constructed a bilayer hydrogel scaffold mimicking the periosteal structure to simultaneously induce neurovascular regeneration and osteogenesis, thereby enhancing bone regeneration and remodeling.¹⁰ However, current neurovascularized engineered bone repair materials are still in the initial stages.

To develop ideal bone repair materials, angiogenesis and innervation should be considered to better reproduce the bone tissue microenvironment. By integrating surrounding tissues through a neurovascular network to provide a biomimetic microenvironment for the stem cells, neurovascularized bone grafts may be more effective in repairing bone defects. In this study, we designed functionalized hydrogel-microsphere composites (RIBQ) for bone defect repair (Fig. 1). RGD peptide and macroporous structure produced by the degradation of GMS promoted the adhesion and spreading of stem cells. BFP-1-

laden MSNs (BFP-1@MSNs) delivered BFP-1 to promote the osteogenic differentiation of stem cells, and the QK-loaded gelatin microspheres (QK/GM) slowly released QK peptide to recruit ECs. IK19 peptide grafted on alginate was beneficial for neuronal growth. In addition, the relationship and the underlying mechanism between nerves, blood vessels, and osteogenesis were preliminarily studied, providing a theoretical basis for the subsequent development of neurovascularized bone repair materials (Table 1).

2 Results and discussion

2.1 Functionalized alginate hydrogel promotes neurite outgrowth

To investigate the effects of alginate hydrogels grafted with RGD and IK19 on the neurons, the morphology of neurons on the hydrogels was observed by IF staining. β -tubulin is required for neuronal axon guidance and maturation and is a

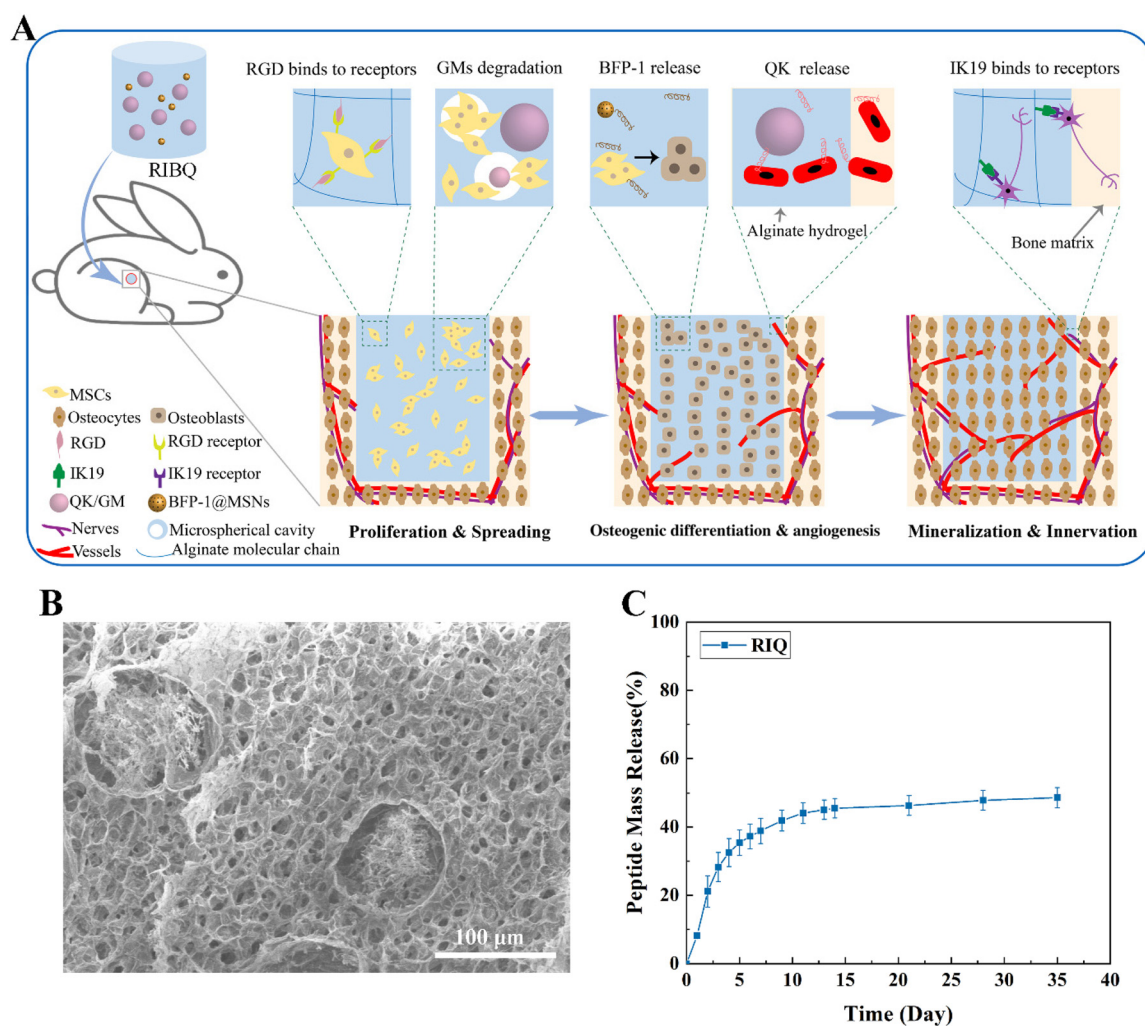


Fig. 1 Schematic diagram of the experimental design and characterization of neurovascularized bone repair system (RIBQ). (A) Experimental schematic of the neurovascularized bone repair system (RIBQ). (B) Scanning electron microscopy (SEM) image of GMS degraded in the alginate hydrogel for 7 days. (C) The sustained release profile of QK peptide in QK/GM-loaded alginate hydrogel.

Table 1 Abbreviations and the preparation of hydrogel

Abbreviation	Description
RA	RGD peptide grafted alginate hydrogel
IA	IK19 peptide grafted alginate hydrogel
RI (RI11)	Hydrogel prepared by mixing RA and IA (1 : 1)
RIQ	RI loaded with QK/GM
RB	RA loaded with BFP-1@MSNs
RIB	RI loaded with BFP-1@MSNs
RIBQ	RI loaded with BFP-1@MSNs and QK/GM

major neuronal marker.¹¹ Cells on RA and RI21 (RA : IA = 2 : 1) expressed β 3-tubulin, but did not have significant neurite outgrowth (Fig. 2A). When the proportion of IK19 in the hydrogel was increased, the cells had neurite outgrowth. However, cells on RI12 (RA : IA = 1 : 2) and IA only formed short neurites, which wrapped around the cell body without fully extending. Neurons on the RI11 extended longer axons to connect with

surrounding cells, suggesting that this hydrogel was more suitable for neuronal axon extension.

Since the RGD peptide can promote cell adhesion, some studies have also used RGD to modify neural scaffolds to improve their function.¹² When Farrukh *et al.* prepared bifunctional hydrogels that enhanced neurogenesis, they found that the number of neurites and axonal length were significantly reduced after replacing IK19 with RGD, indicating that the peptides with the IKVAV sequence may be more conducive to neuronal growth.¹³ IKVAV exists in the α -chain globular region of laminin-1, which is a major component of the basal layer of peripheral nerves and plays an important role in the neurite outgrowth.^{14,15} Some studies have combined RGD and IKVAV to prepare hydrogels for nerve repair, such as designing nanofibrous hydrogels containing IKVAV and RGD to improve the neuronal microenvironment to promote nerve regeneration.¹⁶ The conjugation of biomimetic peptides in hydrogels promoted stem cell differentiation and tissue regeneration.^{17,18}

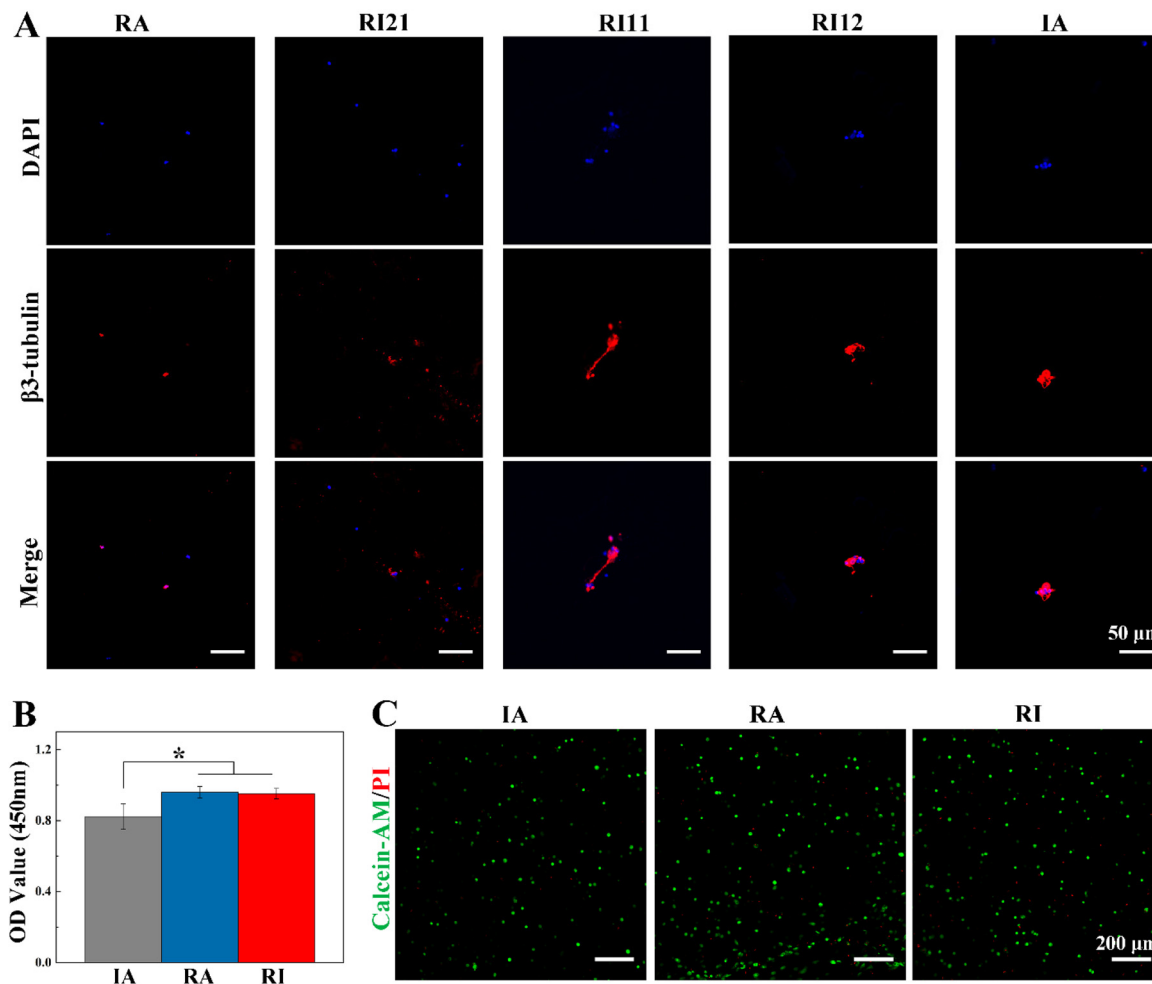


Fig. 2 Evaluation of cell viability of different peptide-modified alginate hydrogels. (A) Immunofluorescence staining images of neurons cultured on the hydrogel surface for 5 days, DAPI (blue), β 3-tubulin (red). Scale bar, 50 μ m. (B) CCK-8 results of hMSCs cultured in IA, RA, and RI (RI11) for 7 days, * $p < 0.05$. (C) Live/dead staining images of hMSCs cultured in different hydrogels for 3 days, Calcein-AM labeled live cells (green), PI labeled dead cells (red). Scale bar, 200 μ m. All data represent means \pm SD ($n = 3$). RA represents RGD peptide grafted alginate hydrogel; IA represents IK19 peptide grafted alginate hydrogel; RI11 represents hydrogel prepared by mixing RA and IA (1 : 1).

Herein, RGD and IK19 peptides are covalently grafted onto sodium alginate molecular chains, which are slowly released with the degradation of the hydrogel, ensuring the long-term residence of the peptides in the hydrogel and forming an osteogenic microenvironment that promotes cell adhesion, proliferation and nerve growth.^{19,20}

2.2 Cell viability of human mesenchymal stem cells (hMSCs) in RI

RGD peptide on alginate hydrogels can bind to integrin receptors on the cell surface to promote cell adhesion and proliferation.¹⁹ IK19 peptide can also bind to integrin receptors, but whether the introduction of IK19 into the hydrogel affects the activity of hMSCs still needs to be explored. The optical density (OD) values of the RI (RI11) and RA groups were similar and not significantly different (Fig. 2B). However, the OD value of IA was slightly lower than those of RA and RI. Although IK19 peptide is based on the IKVAV pentapeptide by introducing charged side chain amino acids to reduce the formation of amyloid fibrils, IK19 solution (0.2 mM) still formed aggregates of ~400 nm, while IKVAV formed aggregates larger than 1 μm .²¹ The formation of these aggregates resulted in a lower density of peptides on the surface of the material, which might affect cell adhesion.

The effect of IK19 on stem cell viability was verified by using live/dead staining. The cells in the three groups of hydrogels were mainly live cells and very few dead cells, indicating that the peptide-modified hydrogels have good cytocompatibility (Fig. 2C). No significant difference was found between RA and RI. Thus, RI can be used for subsequent studies to promote the growth of neurons without reducing the 3D culture activity of the stem cells.

2.3 Osteogenesis and neurovascularization of hMSCs-loaded RIBQ *in vivo*

Different cell-laden alginate hydrogels were transplanted subcutaneously into nude mice (Fig. S1A†), and samples were harvested after 4 weeks to analyze the mineralization results. Although the volume of the newly formed bone was slightly higher in RI than in RA, no statistical difference was found between the RA and RI groups (Fig. 3A and B). The bone mineralization effects of RB, RIB and RIQ were obvious, but no significant difference among the three hydrogels was found. The results from quantitative analysis showed that RIBQ had the best *in vivo* osteogenic differentiation effect (Fig. 3B), which may be mainly due to the effect of QK/GM and BFP-1 in promoting the osteogenic differentiation of hMSCs.⁵

To further explore the osteogenic differentiation effect of the hydrogel *in vivo*, Masson staining and immunohistochemical (IHC) staining were performed. RB, RIB, RIQ and RIBQ had more collagen deposition compared with RA and RI. This was mainly due to the sustained release of BFP-1 in the hydrogels that promoted the osteogenic differentiation of hMSCs, and on the other hand, the macroporous structure produced by the degradation of GMs was conducive to cell aggregation and promoted type I collagen secretion. The IHC

staining and quantitative analysis of osteogenic proteins (Fig. 3C and S2B†) showed that the OCN expression was the weakest in RA and gradually increased in RI and RIQ, while the OCN expression was not significantly different in RIQ, RB and RIB and was lower than that in RIBQ. These results suggest that during new bone formation, a neurovascularized osteogenic microenvironment is developed through the promotion of vascular and neural infiltration by QK and IK19 peptides, which is more conducive to bone matrix secretion and mineralization than that by the osteogenic peptide BFP-1. The results of *in vitro* experiments showed that the introduction of the IK19 peptide into the alginate hydrogel was beneficial for the extension of the neuronal axons. Whether the RIBQ hydrogel-microsphere composites could facilitate nerve fiber infiltration *in vivo* was explored by IF staining and quantitative analysis (Fig. 3E and S2A†). Little β 3-tubulin expression was found in RA and RB, while β 3-tubulin was expressed at the edges of RI, RIB, RIQ, and RIBQ, suggesting that the hydrogels containing IK19 favored the infiltration of neurons. In addition, the β 3-tubule expression in RIQ was higher than in RI and RIB but lower than in RIQB, suggesting that angiogenesis and neural infiltration go hand in hand during osteogenesis.

The previous research results have confirmed that RBQ can promote angiogenesis *in vivo*.⁵ To explore whether the introduction of IK19 into the hydrogel will affect angiogenesis *in vivo*, hematoxylin and eosin (H&E) staining was performed. RA and RB had angiogenesis at the edge of the hydrogel, mainly due to the effect of the RGD peptide (Fig. 3D). In RI and RIB, blood vessels were found at the edge and periphery of the hydrogel, which were more abundant than those in RA and RB, indicating that the introduction of IK19 was beneficial for angiogenesis *in vivo*. Studies have shown that perivascular nerves may secrete neuropeptides (*e.g.*, VIP) to stimulate the proliferation and migration of ECs, thereby promoting angiogenesis.⁷ The ingrowth of neurons guided by IK19 in RI and RIB might be beneficial for angiogenesis, but this inference requires further validation. There were also dense blood vessels inside the hydrogels of RIQ and RIBQ, mainly due to the sustained release of QK peptide, which recruited endogenous ECs and promoted angiogenesis. This indicated that the transplantation of cell-loaded RIBQ realized the coordinated effect of hydrogel, stem cells and bioactive factors, which together promoted osteogenesis and neurovascularization.

2.4 RIBQ promoted the repair of *in situ* bone defects

To investigate whether the neurovascularized alginate hydrogel could effectively repair bone defects, a New Zealand white rabbit femoral defect model was prepared (Fig. S1B†). The hydrogel was filled into the defect, and the samples were harvested after one month. A layer of bone tissue was observed on the surface of the control group (Defect), but almost no new bone formed inside the defect (Fig. 4A). This indicated that the bone tissue had a certain self-repairing ability, but the repairing ability was limited. Thus, additional interventions were necessary to promote bone defect repair. After the implantation of cell-laden RA (RA/C) in the defect, in addition

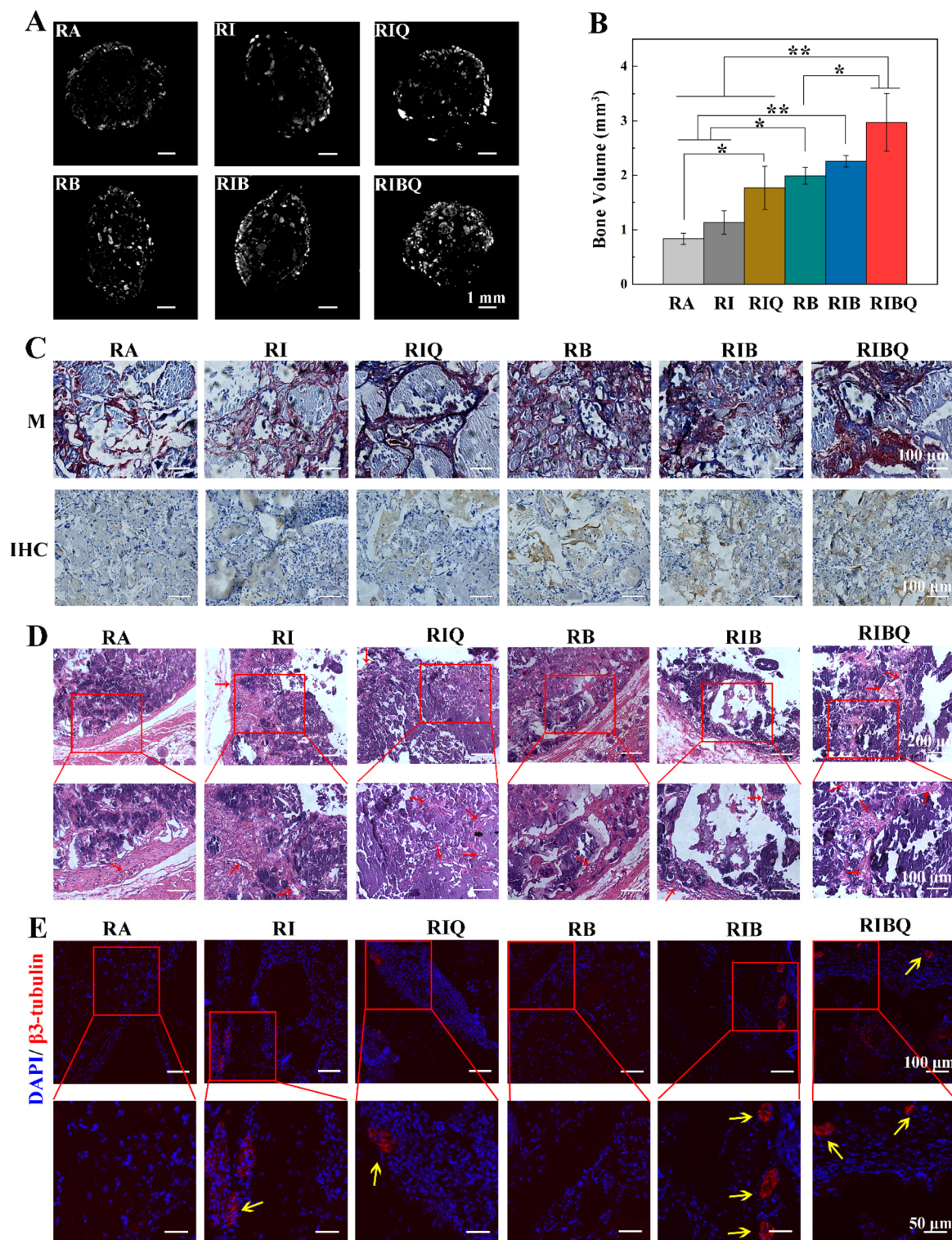


Fig. 3 Bone regeneration and neurovascular regeneration after 4 weeks of subcutaneous transplantation in mice. (A) Micro-CT reconstruction image. (B) Quantitative analysis of bone mineralization volume; * $p < 0.05$ and ** $p < 0.01$. (C) Masson (M) staining and IHC staining (OCN) images, scale bar, 100 μm . (D) H&E staining results, red arrows: blood vessels. (E) Immunofluorescence staining image, DAPI (blue), β 3-tubulin (red), yellow arrows: nerve. All data represent means \pm SD ($n = 3$). RA represents RGD peptide grafted alginate hydrogel; RI represents hydrogel prepared by mixing RA and IA (1:1); RIQ represents RI loaded with QK/GM; RB represents RA loaded with BFP-1@MSNs; RIB represents RI loaded with BFP-1@MSNs; RIBQ represents RI loaded with BFP1@MSNs and QK/GM.

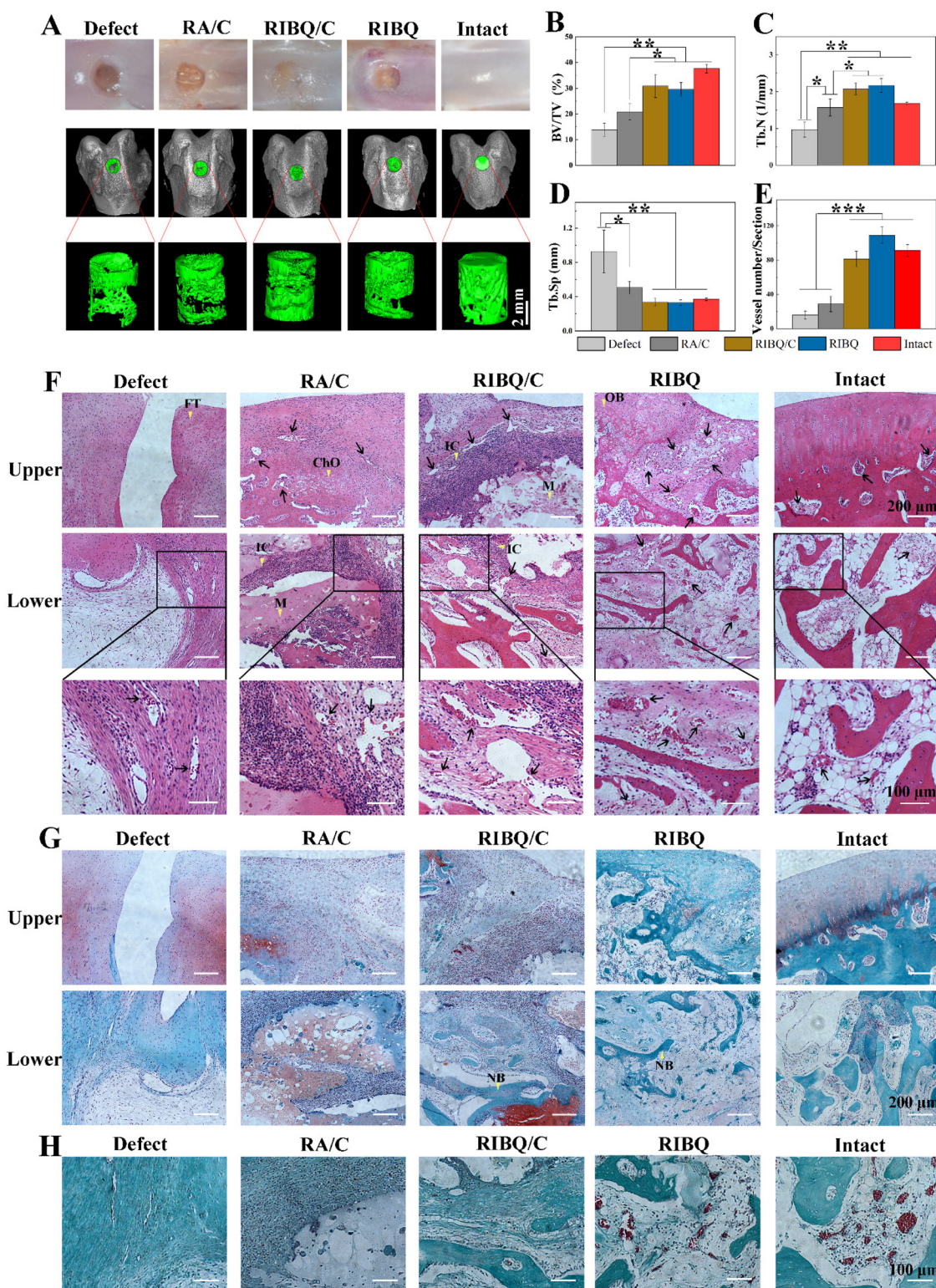


Fig. 4 Evaluation of bone repair in the rabbit femoral defect. (A) Photograph and micro-CT 3D reconstruction of the femur one month after surgery. (B–D) Quantitative histomorphometry analyses of bone regeneration (BV/TV, the bone volume fraction; Tb-N, the bone trabecular number; Tb-Sp, the bone trabecular separation). (E) Quantitative analysis of vessel number in the defect area. (F) H&E staining images of the superficial and underlying layers of the defect. Scale bar, 200 μm . (G) Safranin O-fast green staining images of the superficial and underlying layers of the defect. Scale bar, 200 μm . (H) Goldner staining images of the underlying layers of the defect. Scale bar, 100 μm . * $p < 0.05$, ** $p < 0.01$, and *** $p < 0.001$. Black arrows, vessels. FT, fibrous tissue; Cho, chondrocyte; IC, immune cells; M, undegraded materials; OB, osteoblasts; NB, new bone. All data represent means \pm SD ($n = 3$). Defect represents defect alone with no treatment; RA/C represents RMSCs-laden RA; RIBQ/C represents RMSCs-laden RIBQ; RIBQ represents RI loaded with BFP-1@MSNs and QK/GM.

to the formation of new bone on the surface, there was also a small amount of bone tissue inside the defect. However, in the RIBQ/C (cell-laden RIBQ) group, more bone tissue was generated in the depth of the defect, filling the defect cavity, similar to the healthy group (Intact). After RIBQ implantation, new bone formed both on the surface and inside the defect, although the bottom of the defect was not completely repaired.

By the quantitative analysis of micro-CT results, the bone volume fraction (BV/TV) of the RIBQ/C, RIBQ, and Intact groups increased significantly compared with that of the Defect group, and the trabecular spacing (Tb-Sp) was significantly reduced (Fig. 4B–D). After implanting RIBQ/C or RIBQ, the trabecular number (Tb-N) increased significantly, indicating that RIBQ could promote bone regeneration, and effectively repair bone defects. However, there was no significant difference in bone mineral density (BMD) and trabecular thickness (Tb-Th) between the RA/C, RIBQ, RIBQ/C and Defect groups, and there were significant differences between these 4 groups and the healthy group (Fig. S3A and B†). Due to the large size of the bone defect and the short time for osteogenic repair, the bone defect area underwent more new bone production than bone remodeling in this short period of one month.^{22–24} The normal bone repair process lasts for several months, and the new bone tissue in this study may not be fully mature during one month. The formed bone tissue was different from that of the normal femur, and the repair time should be extended in the follow-up.

Many studies have reported the good repairing effect of hydrogels in bone defects. Zhang *et al.* used gold nanoparticle-loaded PEG hydrogels in rabbit femoral defects (4 mm in diameter and 3 mm in depth). Micro-CT analysis at 8 weeks after surgery showed a BV/TV of 26.4% in the experimental group compared to 11.0% in the defect group.²⁵ Sarker *et al.* implanted an oxidized alginate–gelatin–biphase calcium phosphate hydrogel composite containing hydroxyapatite particles into a rabbit femoral defect (8 mm in diameter and 5 mm in depth). The BV/TV was approximately 20% (5% in the defect group), and the BV/TV at 8 weeks reached 37%, showing accelerated bone defect repair.²⁶ In this study, RIBQ was implanted in the defect (4 mm in diameter and 5 mm in depth) for one month, and the BV/TV reached 30%, which was close to that of the healthy bone tissue.

Histological staining was performed to further analyze the structure of the new bone tissue in the defect. The results of H&E staining showed the cells crawling out of the adjacent normal bone tissue at the edge of the defect differentiated into chondrocytes, but there were obvious defect cavities in the Defect group, indicating that self-repair could not be achieved within one month (Fig. 4F and S3C†). A layer of fibrous tissue with few blood vessels formed at the surface of the defect, and connective tissue deep within the defect was found (Fig. 4G and H). Bone tissue repair undergoes inflammation and hematoma, and the clotted blood is replaced by fibrous tissue and cartilaginous callus, which transforms into a hard callus and eventually forms mature bone tissue.²⁷ In the RA/C group,

some vascular infiltration and cartilage formation were observed on the surface of the defect, and there are some immune cells deep in the defect caused by the implanted rabbit mesenchymal stem cells (RMSCs), and these allogeneic cells showed a certain immune rejection (Fig. 4F and G). In the RIBQ/C group, immune cells were also noted, but mineralized bone tissue and red cartilage tissue formed in the depth of the defect, with abundant blood vessels in the whole new tissue (Fig. 4F–H). The red cartilage had not yet mineralized into a hard callus, indicating that it was repaired by endochondral osteogenesis. After implantation of the RIBQ, there were abundant blood vessels throughout the nascent tissue, including deep within the defect (Fig. 4F). The superficial layer of the defect had osteoblasts and mineralized bone tissue, and part of the new bone tissue deep in the defect. Healthy bone tissue had a layer of chondrocytes on the surface, and inside was mature mineralized bone tissue surrounded by abundant blood vessels (Fig. 4F–H). Quantitative analysis of blood vessels in the defect area showed that the number of blood vessels in the RIBQ/C and RIBQ groups was similar to that of the normal bone tissue, and was significantly higher than that in the Defect and RA/C groups (Fig. 4E). This was mainly due to the release of QK peptide in the hydrogel to promote angiogenesis, and these new blood vessels could supply oxygen and nutrients to the bone tissue, which might be beneficial for bone repair.

Immunofluorescence staining images and quantitative analysis (Fig. 5 and S4†) showed that β 3-tubulin was not expressed in the deep defect of the Defect and RA/C groups, but CD31 (the marker of blood vessels) was expressed. The expression of β 3-tubulin and CD31 could be observed in both the RIBQ and RIBQ/C groups, indicating that the neurovascularized hydrogel–microsphere composites promoted the ingrowth of blood vessels and nerve fibers. IF staining results of the healthy tissue also confirmed that bone tissue is a highly neurovascularized tissue. β 3-tubulin and CD31 were found to merge in some areas, suggesting a similar distribution of blood vessels and nerves in the new bone tissue. The above results indicated that the neurovascularized hydrogel–microsphere composite RIBQ not only promoted the repair of bone defects, but also facilitated angiogenesis and nerve fiber infiltration, which might be beneficial for restoring the structure and function of bone tissue.

2.5 Preliminary study on the relationship of ECs, neurons, and bone lineage cells

Although researchers have recently paid more attention to the bone regeneration of neurovascularization, the relationships between blood vessels, nerves, and bone regeneration remain unclear. The *in vivo* results suggested a connection between nerve fiber growth and angiogenesis, especially in new bone tissue, where blood vessels and nerve distribution are highly coupled. Previous studies have inferred that osteoblasts and neurons may secrete some bioactive factors for signal transduction and regulation.²⁸ In this study, by collecting the conditioned medium (CM), the influence and mechanism of

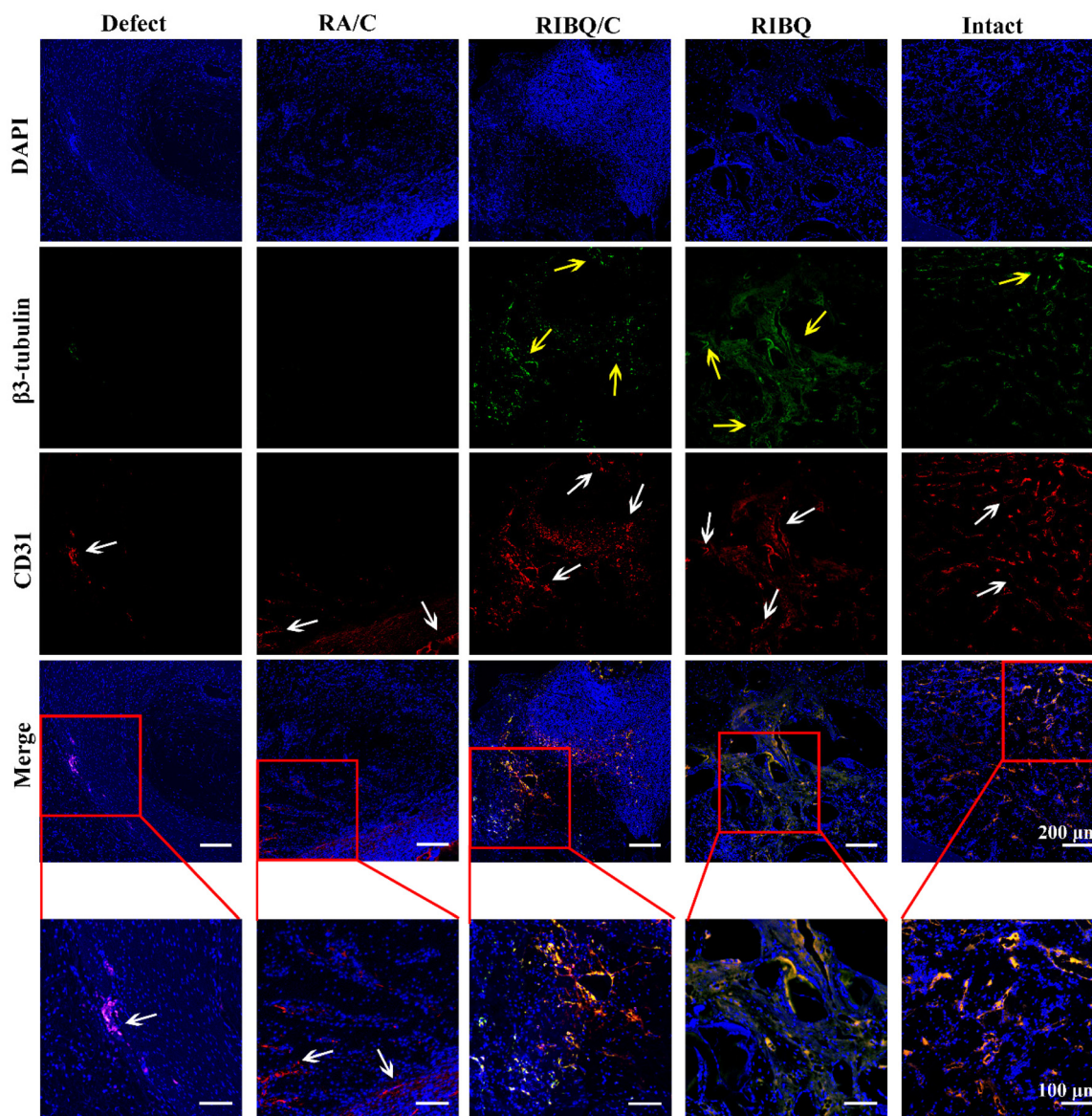


Fig. 5 Neurovascular assessment in new formed tissue at the defect site. Immunofluorescence staining images, DAPI (blue) labeled nuclei, CD31 (red) labeled blood vessels (white arrows), β 3-tubulin (green) labeled nerves (yellow arrows). Defect represents defect alone with no treatment; RA/C represents RMSCs-laden RA; RIBQ/C represents RMSCs-laden RIBQ; RIBQ represents RI loaded with BFP-1@MSNs and QK/GM.

osteoblasts and neurons on ECs were preliminarily discussed. The hMSCs differentiated into osteoblasts, and the CM was beneficial for the healing of scratches, indicating that the osteoblasts may secrete bioactive factors to stimulate the migration of human umbilical vein endothelial cells (HUVECs) (Fig. 6A). CCK-8 assay results showed that osteoblast CM (DMEM-CM) significantly promoted the proliferation of HUVECs (Fig. 6B). The neuronal conditioned medium (NM-CM) promoted the proliferation and migration of HUVECs (Fig. 6A and B).

To clarify the signaling pathways affecting the HUVECs, the expression of differential genes was analyzed by the Kyoto Encyclopedia of Genes and Genomes (KEGG). Compared with

DMEM, the differential genes of DMEM-CM were mainly enriched in PI3K/Akt and MAPK signaling pathways and manifested in significant differences in focal adhesions, cell adhesion molecules, extracellular matrix (ECM), cytokines and microRNAs, *etc.* (Fig. 6C and S5A[†]). Bone cell lineage (such as hypertrophic chondrocytes and osteoblasts) can interact with vascular cells, regulate the production of angiogenic factors (such as VEGF) and stimulate neovascular infiltration in tissues.²⁹ The binding of VEGF to VEGFR activates the MAPK pathway, specifically the phosphorylation of ERK1/2, which reorganizes actin and stimulates cell migration.³⁰ In addition to the MAPK pathway, VEGF can also activate the PI3K/Akt pathway, which stimulates the proliferation and migration of

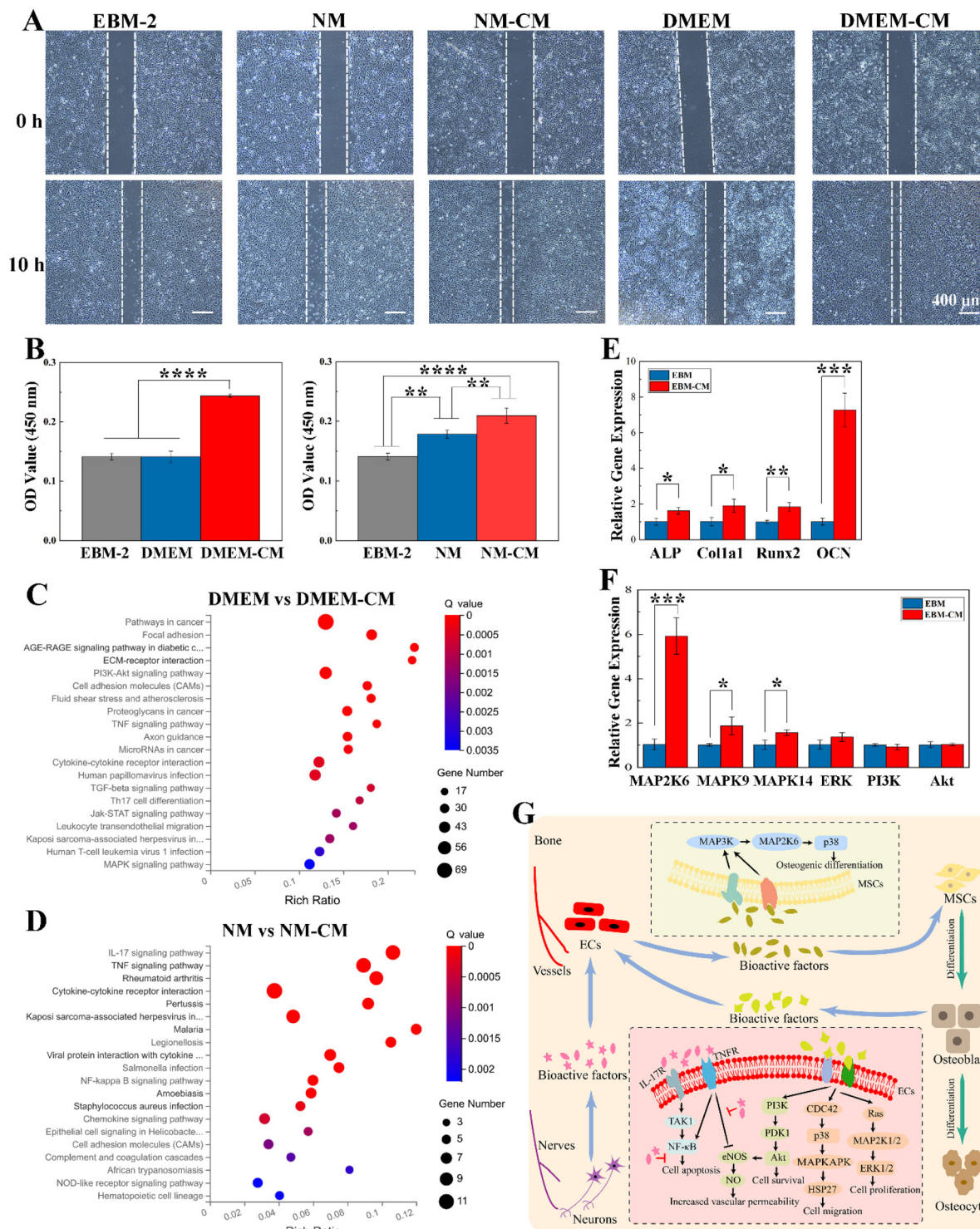


Fig. 6 Preliminary study on the relationship of ECs, neurons and bone lineage cells. (A) Micrograph of the cell scratch experiment, scale bar, 400 μ m. (B) CCK-8 results of HUVECs cultured in osteoblast conditioned medium (DMEM-CM) or neuronal conditioned medium (NM-CM) for 3 days. (C) KEGG analysis between DMEM and DMEM-CM. (D) KEGG analysis between NM and NM-CM. (E) qRT-PCR analysis of osteo-related genes. (F) qRT-PCR analysis of pathway-related genes. (G) Schematic representation of the relationship between nerves, blood vessels, and osteogenesis in bone tissue. * $p < 0.05$, ** $p < 0.01$, *** $p < 0.001$, and **** $p < 0.0001$.

ECs. Although ERK/MAPK pathway activation can induce angiogenesis, such a process cannot induce vascular permeability, while the activation of PI3K is necessary for angio-

genesis and vascular permeability.³¹ In addition to VEGF, epidermal growth factor, angiopoietin 1, *etc.* can also stimulate angiogenesis through the MAPK and PI3K pathways.

Therefore, the components of the bioactive factors secreted by osteoblasts remain to be further investigated.

The analytical results of KEGG showed that compared with NM, the differential genes of NM-CM were mainly enriched in the IL-17 and TNF signaling pathways, which were manifested in significant differences in cell adhesion molecules and cytokines (Fig. 6D and S5B†). Interleukin-17 (IL17) promotes the inflammatory phenotype through NF- κ B activation, and it has also been reported to regulate downstream target genes associated with angiogenesis.³² Tumor necrosis factor alpha (TNF α) is a pro-inflammatory factor with dual pro-angiogenic and anti-angiogenic properties.³³ TNF α interacts with two distinct transmembrane receptors (TNFR1 and TNFR2), and TNF α /TNFR2 is involved in cell survival and pro-angiogenesis. In contrast, TNF α /TNFR1 activates NF- κ B, leading to cellular inflammation and apoptosis.³⁴ The activation of TNFR1 also stimulates ROS production, thereby reducing available NO, which is a key determinant of vascular responsiveness.³⁵ The above results showed that NM-CM promoted the proliferation and migration of HUVECs. However, the expression of inflammation-related genes was downregulated, indicating that neurons secreted bioactive factors to inhibit the inflammatory signaling pathway and increase the activity of ECs.

During fracture healing, the relationship between angiogenesis and osteogenesis is very close, and blood vessels in the bone marrow play an important role in both osteogenic and hematopoietic stem cells.³⁶ Xu *et al.* co-cultured mouse endothelial progenitor cells (EPCs) and MSCs, and found that EPCs could enhance the osteogenic differentiation of MSCs by activating the p38 MAPK pathway with the use of microarray technology.³⁷ To further verify the effect of angiogenesis on the osteogenic differentiation of hMSCs, we collected the CM of HUVECs to explore its effect on the osteogenic differentiation of hMSCs. EBM-CM significantly increased the expression of alkaline phosphatase (ALP) activity and osteogenic genes (ALP, Col1a1, Runx2, and OCN), and promoted calcium deposition (Fig. 6E and S6†). IF staining also confirmed that EBM-CM promoted the osteogenic differentiation of hMSCs (Fig. S6C†). The related pathway genes of osteogenic differentiation were detected by quantitative reverse-transcription polymerase chain reaction (qRT-PCR). EBM-CM significantly promoted the expression of MAP2K6, MAPK9 and MAPK14, while the expression of ERK, PI3K and Akt had no statistical difference (Fig. 6F). This result suggested that the bioactive factors secreted by ECs activated MAP3K (such as DLK, TAK, *etc.*), which in turn activated MAP2K6, which led to the phosphorylation of p38 MAPK and enhanced the expression of osteoblast-related transcription factors.³⁸

The above results indicated that both osteoblasts and neurons could secrete bioactive factors to stimulate the proliferation and migration of ECs, and promote angiogenesis by activating multiple pathways. The generated blood vessels could secrete osteogenic factors to promote the osteogenic differentiation of stem cells or progenitor cells, forming a positive feedback (Fig. 6G).

3 Conclusions

In summary, we have designed neurovascularized hydrogel-microsphere composites, which enhanced the neurite outgrowth and angiogenesis in the bone defects, reproduced the bone tissue microenvironment, and improved the repair effect of bone defects. Osteoblasts and neurons secreted bioactive factors that acted on the ECs to promote angiogenesis. The ECs secreted bioactive factors that further enhanced bone regeneration by promoting the osteogenic differentiation of MSCs. Signaling pathways such as PI3K, MAPK, IL-17 and TNF pathways were involved in these processes. This study is of great significance for the development of neurovascularized bone repair materials for clinical application and also provides a theoretical basis and new ideas for subsequent in-depth research.

4 Experimental section

4.1 Preparation of peptide-treated alginate hydrogel

As described previously,¹⁹ RGD peptide (Ac-GGGGRGDASSP-NH₂) or IK19 peptide (Ac-CSRARKQAASIKVAVSADR-NH₂) was grafted onto alginate using the carbodiimide method. Briefly, EDC and sulfo-NHS were reacted with alginate solution in 0.1 M MES buffer to form a stable intermediate, RGD or IK19 peptide was added to the solution, and the resulting mixture was allowed to react at 25 °C for 12 h. The final RGD/IK19 concentration was 1 mM. Following peptide modification, the alginate was dialyzed (3.5 kDa), sterile-filtered (0.22 μ m), and freeze-dried. With the use of luer-lock syringes, the RGD-treated or IK19-treated alginate was mixed with calcium sulfate slurry (1.22 M). Then, the mixture was injected into the mold for cross-linking for 15 min to obtain the RGD-treated alginate hydrogel (RA) or the IK19-treated alginate hydrogel (IA). RGD-treated alginate was mixed with IK19-treated alginate in different volume ratios (2:1, 1:1, and 1:2) and then cross-linked with calcium sulfate to obtain double-peptide-modified hydrogels (*i.e.*, RI21, RI11, and RI12).

4.2 Cell culture

SD rat embryonic cortical neurons (rCNs) were purchased from Cyagen Biosciences Co., Ltd and cultured in a rat neuron complete medium (NM; Cyagen Biosciences Co., Ltd, China). The hydrogel (diameter: 5 mm, height: 1 mm) was placed in an ultra-low-adhesion 96-well plate, and rCNs were seeded on the hydrogel surface for two-dimensional (2D) culture. After the rCNs were incubated for 6 h, the medium was replaced with fresh medium. Human mesenchymal stem cells (hMSCs) were purchased from ScienCell Research Laboratories (USA) and cultured in the growth medium, which was high glucose Dulbecco's modified Eagle's medium (DMEM; Hyclone, USA) supplemented with 10% fetal bovine serum (FBS; Gibco, USA) and 1% penicillin/streptomycin (Gibco). The cells in the dish were trypsinized and resuspended, and the cell suspension

was mixed with alginate solution through luer-lock syringes. Then the cell-laden alginate solution (3×10^6 cells per mL) was mixed with calcium sulfate and injected into the mold. The cell-laden hydrogels were transferred to ultra-low-adhesion 24-well plates, and the growth medium was added to culture for 7 days. Rabbit bone marrow mesenchymal stem cells (RMSCs) were purchased from Cyagen Biosciences Co., Ltd and cultured in the growth medium. The cells were expanded to the fifth passage. RMSC-loaded hydrogel (1×10^7 cells per mL) was prepared in the same way as that of the hMSC-loaded hydrogel.

4.3 Immunofluorescence (IF) staining

The rCNs grown on the hydrogel surface were rinsed with PBS, fixed with 4% paraformaldehyde at room temperature, and permeabilized with 0.1% Triton X-100. The cells were blocked with 3% bovine serum albumin (Sigma-Aldrich) and incubated at 4 °C overnight with β 3-tubulin primary antibody (Abcam, UK). Then, the cells were rinsed with PBS and incubated with secondary antibody for 1 h in the dark. DAPI (10 mg mL^{-1} ; Sigma-Aldrich) was used to stain the nuclei in the dark for 10 min. The cells were observed and photographed using a confocal laser scanning microscope (Nikon, Japan).

4.4 Viability of the hMSCs

The viability of the hMSCs was assessed using the CCK-8 kit (DOJINDO, Japan). After the cells were incubated for 7 days, 10% CCK-8 reagent was added, and OD_{450} was detected using a microplate reader (Molecular Devices, USA). To observe the survival of the hMSCs in the different 3D hydrogels, a live/dead staining kit (Invitrogen, USA) was used for cell staining after 3 days of culture. The cells were photographed using a confocal laser scanning microscope.

4.5 Preparation of alginate hydrogel-based neurovascularized composites (RIBQ)

As reported previously,⁵ GMs were prepared by water-in-oil emulsification and genipin cross-linking. Then, the GMs were incubated with QK peptide (Ac-KLTWQELYQLKYKGI-NH₂) overnight to obtain QK-loaded microspheres (QK/GM). BFP-1 laden MSNs (BFP-1@MSNs) were prepared as described previously.¹⁹ A solution of RA-modified alginate and IK19-modified alginate was mixed in the ratio of 1 : 1, mixed with QK/GM (5 mg mL^{-1}) and BFP-1@MSN (1 mg mL^{-1}), and then cross-linked with calcium sulfate to obtain RIBQ. RB was RA containing BFP-1@MSN (1 mg mL^{-1}). The hydrogels prepared from a 1 : 1 mixture of RA-modified alginate and IA-modified alginate containing BFP-1@MSN (1 mg mL^{-1}) or QK/GM (5 mg mL^{-1}) were RIB or RIQ, respectively.

4.6 *In vivo* transplantation

All animal procedures were performed in accordance with the Guidelines for the Care and Use of Laboratory Animals of Peking University and approved by the Institutional Animal Care and Use Committee of Peking University, China.

4.7 Subcutaneous transplantation in mice

The *in vivo* osteogenic, vascularization and neuralization effects of different hydrogels were evaluated by subcutaneous transplantation in male BALB/c nude mice (6–8 weeks old, SPF grade). As previously described, the hMSCs (1×10^7 cells per mL) were encapsulated into RA, RI, RB, RIB, RIQ, and RIBQ. The cell-loaded hydrogels (diameter: 5 mm, height: 2 mm) were cultured in an osteogenic induction medium for 7 days. The medium consisted of low-glucose DMEM supplemented with 10 mM β -glycerol phosphate, 50 mg mL⁻¹ ascorbic acid and 0.1 mM dexamethasone. The mice were anesthetized by the intraperitoneal injection of sodium pentobarbital, and an incision was made in each mouse on both sides of the back, in which the cell-loaded hydrogel was implanted (Fig. S1A†). Four weeks after implantation, the mice ($n = 10$) were sacrificed, and the implants were collected and fixed in 10% neutral formalin for 48 h.

4.8 Rabbit femoral defect model

Male New Zealand white rabbits (male, 2.5–3.0 kg, 4–5 months old), two experimental animals in each group, and a total of 10 rabbits in five groups, were anesthetized by injection with sodium pentobarbital and lidocaine. A bone defect (4 mm diameter, 5 mm deep) was drilled in the femur. After pressing with a cotton ball to stop the bleeding, the defect was filled with RMSCs-loaded RA (RA/C), RMSCs-loaded RIBQ (RIBQ/C), or RIBQ (Fig. S1B†). The untreated defect was used as a negative control (Defect). To prevent postoperative infection, penicillin (100 000 units per kg) was injected intramuscularly once a day for three consecutive days. The healthy and intact femur was used as a positive control (Intact). One month after surgery, the rabbits were euthanized. The femur was removed and fixed in 10% formalin.

4.9 Micro-computed tomography (CT) and histological analysis

Visualization of mouse subcutaneous implants was performed by micro-CT and quantification of total bone volume in the hydrogels. After the samples were sectioned by paraffin embedding, hematoxylin and eosin (H&E) staining, Masson staining, immunohistochemistry (IHC) staining and IF staining were performed. The harvested rabbit femur samples were visualized by micro-CT and quantified for bone mineral density (BMD), bone volume fraction (BV/TV), trabecular thickness (Tb·Th), trabecular spacing (Tb·Sp), and trabecular number (Tb·N). After the samples were decalcified by ethylenediamine tetraacetic acid, paraffin-embedded sections were performed, followed by H&E staining, Safranin O-fast green staining, Goldner staining and IF staining.

4.10 Assessment of the relationship between ECs, neurons and bone lineage cells

Indirect co-cultures were performed using the conditioned medium (CM) transfer method as reported previously.^{39,40} Human umbilical vein endothelial cells (HUVECs) were pro-

vided by Zhao Yang Laboratory of Peking University, and cultured in endothelial basal media-2 (EBM-2; Lonza) for 48 h. The supernatant was collected by centrifugation as the EC conditioned medium (EBM-CM). After 14 days of osteogenic induction of the hMSCs in six-well plates, low-glucose DMEM was added and cultured for 48 h. The medium was centrifuged, and the supernatant was collected as the osteoblast conditioned medium (DMEM-CM). The rCNs were cultured for 48 h, and the supernatant was collected after centrifugation as the neuron conditioned medium (NM-CM). To explore whether osteoblasts and rCNs secrete bioactive factors to affect the activity of HUVECs, we stimulated HUVECs by adding different media and performed CCK-8 assay and scratch experiments. The different groups were as follows: (1) EBM group: EBM-2; (2) DMEM group: DMEM and EBM-2 at 1 : 1; (3) DMEM-CM: DMEM-CM and EBM-2 at 1 : 1; (4) NM group: NM and EBM-2 at 1 : 1; and (5) NM-CM group: NM-CM and EBM-2 at 1 : 1. To further explore the mechanism by which CM affects the activity of HUVECs, the RNA of the HUVECs was also extracted. Transcriptome sequencing (RNA-seq) analysis was performed on the Illumina Hiseq platform. To explore whether HUVECs secrete bioactive factors that affect the osteogenic differentiation of hMSCs, osteogenic induction medium and EBM or EBM-CM in a ratio of 1 : 1 were added to stimulate hMSCs for 14 days. Alkaline phosphatase (ALP) activity assessment, Alizarin Red staining, IF staining and quantitative reverse-transcription polymerase chain reaction (qRT-PCR) were performed.

4.11 Statistical analysis

The data were expressed as mean \pm standard deviation and statistically analyzed using Origin 2019 software. Differences between the groups were analyzed by one-way analysis of variance (ANOVA) and Tukey's test. $P < 0.05$ was considered to be statistically different.

Conflicts of interest

All authors declare no conflicts of interest in this work.

Acknowledgements

We thank the National Center for Protein Sciences at Peking University in Beijing, China, for assistance with instruction on using the confocal laser scanning microscope and qRT-PCR instrument. We thank Professor Yang Zhao (Institute of Molecular Medicine, Peking University) for providing HUVECs. We thank the Xiaodong Su laboratory (School of Life Science, Peking University) for their help in conducting the cell experiments. This work was supported by the National Natural Science Foundation of Jiangsu Province (BK20141141) and special funds on the Regenerative Innovation of PKU AAIS-HGB Program.

References

- 1 S. Stegen, N. van Gastel and G. Carmeliet, *Bone*, 2015, **70**, 19–27.
- 2 N. G. Schott, N. E. Friend and J. P. Stegemann, *Tissue Eng., Part B*, 2021, **27**, 199–214.
- 3 M. I. Santos and R. L. Reis, *Macromol. Biosci.*, 2010, **10**, 12–27.
- 4 T. Rademakers, J. M. Horvath, C. A. van Blitterswijk and V. L. S. LaPointe, *J. Tissue Eng. Regener. Med.*, 2019, **13**, 1815–1829.
- 5 Q. Li, H. Zhang, J. Pan, B. Teng, Z. Zeng, Y. Chen, Y. Hei, S. Zhang, S. Wei and Y. Sun, *J. Mater. Chem. B*, 2021, **9**, 6056–6067.
- 6 J.-j. Fan, T.-w. Mu, J.-j. Qin, L. Bi and G.-x. Pei, *BioMed Res. Int.*, 2014, **2014**.
- 7 A. Marrella, T. Y. Lee, D. H. Lee, S. Karuthedom, D. Syla, A. Chawla, A. Khademhosseini and H. L. Jang, *Mater. Today*, 2018, **21**, 362–376.
- 8 Q.-Q. Wan, W.-P. Qin, Y.-X. Ma, M.-J. Shen, J. Li, Z.-B. Zhang, J.-H. Chen, F. R. Tay, L.-N. Niu and K. Jiao, *Adv. Sci.*, 2021, **8**(7), 2003390.
- 9 L. Feng, E. Lingling and H. Liu, *Biomed. Pap.*, 2015, **159**, 637–641.
- 10 Y. Xu, C. Xu, L. He, J. Zhou, T. Chen, L. Ouyang, X. Guo, Y. Qu, Z. Luo and D. Duan, *Bioact. Mater.*, 2022, **16**, 271–284.
- 11 C. D. Katsetos, A. Legido, E. Perentes and S. J. Mork, *J. Child Neurol.*, 2003, **18**, 851–866.
- 12 X. Tang, X. Gu, T. Huang, X. Chen, Z. Zhou, Y. Yang and J. Ling, *ACS Macro Lett.*, 2021, **10**, 1501–1509.
- 13 A. Farrukh, F. Ortega, W. Fan, N. Marichal, J. I. Paez, B. Berninger, A. del Campo and M. J. Salierno, *Stem Cell Rep.*, 2017, **9**, 1432–1440.
- 14 W.-L. Lei, S.-G. Xing, C.-Y. Deng, X.-C. Ju, X.-Y. Jiang and Z.-G. Luo, *Cell Res.*, 2012, **22**, 954–972.
- 15 J. E. Frith, R. J. Mills, J. E. Hudson and J. J. Cooper-White, *Stem Cells Dev.*, 2012, **21**, 2442–2456.
- 16 Y. Sun, W. Li, X. Wu, N. Zhang, Y. Zhang, S. Ouyang, X. Song, X. Fang, R. Seeram, W. Xue, L. He and W. Wu, *ACS Appl. Mater. Interfaces*, 2016, **8**, 2348–2359.
- 17 R. Li, S. Lin, M. Zhu, Y. Deng, X. Chen, K. Wei, J. Xu, G. Li and L. Bian, *Sci. Adv.*, 2019, **5**, eaaw3896.
- 18 Y. Deng, R. Li, H. Wang, B. Yang, P. Shi, Y. Zhang, Q. Yang, G. Li and L. Bian, *ACS Nano*, 2021, **16**, 1051–1062.
- 19 Z. Luo, S. Zhang, J. Pan, R. Shi, H. Liu, Y. Lyu, X. Han, Y. Li, Y. Yang, Z. Xu, Y. Sui, E. Luo, Y. Zhang and S. Wei, *Biomaterials*, 2018, **163**, 25–42.
- 20 H. Zhang, Q. Li, X. Xu, S. Zhang, Y. Chen, T. Yuan, Z. Zeng, Y. Zhang, Z. Mei and S. Yan, *ACS Appl. Mater. Interfaces*, 2022, **14**, 52599–52617.
- 21 A. Farrukh, S. Zhao, J. I. Paez, A. Kavyanifar, M. Salierno, A. Cavalie and A. del Campo, *ACS Appl. Mater. Interfaces*, 2018, **10**, 41129–41137.
- 22 S. Stewart, S. J. Bryant, J. Ahn and K. D. Hankenson, in *Translational regenerative medicine*, Elsevier, 2015, pp. 313–333.

- 23 P. Kolar, K. Schmidt-Bleek, H. Schell, T. Gaber, D. Toben, G. Schmidmaier, C. Perka, F. Buttgereit and G. N. Duda, *Tissue Eng., Part B*, 2010, **16**, 427–434.
- 24 L. Claes, S. Recknagel and A. Ignatius, *Nat. Rev. Rheumatol.*, 2012, **8**, 133–143.
- 25 Y. Zhang, P. Wang, H. Mao, Y. Zhang, L. Zheng, P. Yu, Z. Guo, L. Li and Q. Jiang, *Mater. Des.*, 2021, **197**, 109231.
- 26 A. Sarker, J. Amirian, Y. K. Min and B. T. Lee, *Int. J. Biol. Macromol.*, 2015, **81**, 898–911.
- 27 M. Ansari, *Prog. Biomater.*, 2019, **8**, 223–237.
- 28 Y. Li, D. Fraser, J. Mereness, A. Van Hove, S. Basu, M. Newman and D. S. W. Benoit, *ACS Appl. Bio Mater.*, 2022, **5**, 20–39.
- 29 C. E. Clarkin and L. C. Gerstenfeld, *Cell Biochem. Funct.*, 2013, **31**, 1–11.
- 30 B. Miller and M. K. Sewell-Loftin, *Front. Cardiovasc. Med.*, 2022, **8**, 804934.
- 31 J. Karar and A. Maity, *Front. Mol. Neurosci.*, 2011, **4**, 51.
- 32 M. L. Carbone and C. M. Failla, *Vasc. Biol.*, 2021, **3**, R96–R105.
- 33 Q. Liang, M. Chalamaiah, W. Liao, X. Ren, H. Ma and J. Wu, *J. Funct. Foods*, 2020, **64**, 103598.
- 34 S. Naserian, M. E. Abdelgawad, M. A. Bakshloo, G. Ha, N. Arouche, J. L. Cohen, B. L. Salomon and G. Uzan, *Cell Commun. Signaling*, 2020, **18**, 596831.
- 35 H. Lin, X. Wu, Y. Yang, Z. Wang, W. Huang, L.-F. Wang, Q.-W. Liu, X.-H. Guan, K.-Y. Deng, T.-S. Li, Y. Qian and H.-B. Xin, *Can. J. Physiol. Pharmacol.*, 2021, **99**, 803–811.
- 36 M. V. Gomez-Gaviro, R. Lovell-Badge, F. Fernandez-Aviles and E. Lara-Pezzi, *J. Cardiovasc. Transl. Res.*, 2012, **5**, 618–630.
- 37 C. Xu, H. Liu, Y. He, Y. Li and X. He, *Stem Cell Res. Ther.*, 2020, **11**, 1–13.
- 38 A. Cuadrado and A. R. Nebreda, *Biochem. J.*, 2010, **429**, 403–417.
- 39 S. Hori, S. Ohtsuki, K. Hosoya, E. Nakashima and T. Terasaki, *J. Neurochem.*, 2004, **89**, 503–513.
- 40 Y. N. Jiang, J. Zhao, F. T. Chu, Y. Y. Jiang and G. H. Tang, *Biol. Open*, 2018, **7**, bio032482.